Responses of Global Atmospheric Energy Transport to Idealized Groundwater Conditions in a General Circulation Model

Chia-Wei Lan, Yen-Ting Hwang, Rong-You Chien, Agnès Ducharne, Min-Hui Lo

Responses of Global Atmospheric Energy Transport to Idealized Groundwater Conditions in a General Circulation Model

CHIA-WEI LAN,[a] YEN-TING HWANG,[a] RONG-YOU CHIEN,[a] AGNÈS DUCHARNE,[b] AND MIN-HUI LO[a]

[a] *Department of Atmospheric Sciences, National Taiwan University, Taipei, Taiwan*
[b] *Sorbonne Université, CNRS, EPHE, UMR 7619 Metis, Paris, France*

(Manuscript received 26 September 2020, in final form 17 June 2022)

ABSTRACT: The representation of groundwater dynamics in land surface models and their roles in global precipitation variations has received attention in recent years. Studies have revealed the overall higher soil moisture but rather diverse precipitation changes after incorporating the groundwater component in climate models. However, groundwater effects on large-scale atmospheric energy transport, the fundamental atmospheric variable regulating Earth's climate, have not been explored thoroughly. In this study, a pair of idealized experiments corresponding to contrast globally fixed water table depths by AMIP-type simulations in the Community Earth System Model was conducted. In the wet (shallow water table) experiments, an increased meridional surface temperature gradient makes the mean meridional energy transports and Hadley circulation stronger than dry (deep water table) experiments over the tropics. Such energy transport changes are primarily attributed to the dynamic contribution (intensified Hadley circulation). The wet experiments make the simulated world be like an aquaplanet simulation with less land–sea temperature contrast and the enhancement (reduction) of mean meridional circulation (stationary eddies) energy transports. Furthermore, the South Asian monsoon circulation in the wet experiment shows a southward shift in the premonsoon season (April–June) and slight weakening in the mature phase (July and August). This study explores the impacts of the soil conditions caused by various water table depths on global energy transport and has further implications for climate model developments and experiment designs.

KEYWORDS: Atmosphere-land interaction; Energy transport; Hadley circulation; Soil moisture

1. Introduction

Soil moisture conditions are influenced by many factors, such as atmospheric forcings (e.g., radiation, precipitation variations, atmospheric humidity, and temperature), land-use change, and groundwater variations. The vertical distribution of soil moisture is strongly dependent on water table dynamics. In general, the shallow water table usually results in wet soil conditions and vice versa; meanwhile, changes in the soil moisture memory are not linear to the variations of water table depths (Güntner et al. 2007; Liang et al. 2005; Lo and Famiglietti 2010). Because of its slow variations, the groundwater could affect the soil moisture variations at longer time scales, thus furthering the precipitation, surface water, and energy budget partitioning, and atmospheric circulations through land–atmosphere interactions (DeAngelis et al. 2010; Lo and Famiglietti 2011; Puma and Cook 2010; Wang et al. 2018; Yeh et al. 1984). In contrast, the groundwater's response to climate variations is usually delayed, and how long the delay is depends on the properties and variations of the aquifer and the atmospheric forcings (Chen et al. 2004). Thus, the groundwater has potential impacts on the soil moisture profile, evaporation rate, and surface temperature (Chen and Hu 2004; Gutowski et al. 2002; Liang et al. 2003; York et al. 2002). Besides, the representation of groundwater components in climate models has received attention in recent years, with the groundwater dynamics calculated by using 1) simple conceptual models based on the historical time series (Cooper et al. 1995), 2) empirical models linking the climate variations and the groundwater changes (Chen et al. 2002), and 3) more complicated models derived from streamflow simulation, groundwater storage changes, and near-surface atmospheric variables in general circulation models (Croley and Luukkonen 2003). Furthermore, Zeng and Decker (2009) used the equilibrium soil moisture distribution to fix the deficient numerical solution in the land surface model when the water table below the specified soil layers.

The global rainfall and temperature strongly depend on soil moisture and land evaporation (Milly 1992; Shukla and Mintz 1982; Walker and Rowntree 1977). Seneviratne et al. (2006) pointed out the causality of land–atmosphere interaction and soil memory through atmospheric general circulation model experiments. Soil moisture, albedo, and roughness changes have broad impacts on the local hydrological cycle and large-scale atmospheric circulation that can lead to precipitation changes, although the empirical claims of these phenomena were based on specific regions, climate conditions, and extreme cases (Betts and Silva Dias 2010; Chen et al. 2019; Chou et al. 2001; Koster et al. 2010; Laguë et al. 2019; Lawrence and Vandecar 2015; Lin et al. 2016; Hirsch et al. 2013; Santanello et al. 2018; Seneviratne et al. 2010). These studies have shown the importance of representing shallow groundwater and its interaction with soil moisture in land surface hydrologic simulations. Also, the large-scale circulation can be subjected to different soil wetness conditions (Berg et al. 2017; Kim and

Supplemental information related to this paper is available at the Journals Online website: https://doi.org/10.1175/JCLI-D-20-0753.s1.

Corresponding author: Min-Hui Lo, minhuilo@ntu.edu.tw

DOI: 10.1175/JCLI-D-20-0753.1

Hong 2007; Koster et al. 2016; Lo and Famiglietti 2011; Medvigy et al. 2013; Schneck and Mosbrugger 2011; Snyder 2010; Swann et al. 2012; Werth 2002). Such soil moisture changes might not be confined to small spatial or temporal scales; on the contrary, soil moisture anomalies could cause changes in large-scale atmospheric circulation or planetary waves. For example, Chou et al. (2001) demonstrated that the precipitation location and intensity depend on whether the soil moisture is active in intermediate climate model simulations.

Previous studies have reported the significant widening of Hadley circulation under global warming by using general circulation models and reanalysis datasets (Adam et al. 2014; Held and Soden 2006; Lu et al. 2007; Ma and Xie 2013; Seo et al. 2014). Such widening and weakening Hadley circulation can be partly attributed to reducing the meridional surface temperature gradient (Adam et al. 2014; Levine and Schneider 2011; Williamson et al. 2013; Seo et al. 2014). Geen et al. (2020) also mentioned that circulation intensity and energy transport are associated with gross moist stability. Evans et al. (2012) and Seager et al. (2003) proposed that warmer tropical sea surface temperature (SST) under the El Niño events, increasing the meridional temperature gradient, can induce a narrower, stronger, and equatorward shifting of Hadley circulation; on the contrary, La Niña events are usually linked with a broader, weaker, and poleward shifting of Hadley circulation. Land-use changes can also lead to northward shifts of global precipitation and change circulation intensity. For example, midlatitude afforestation leads to an enhanced meridional temperature gradient, and then the changes in general circulation redistribute the anomalous energy absorbed in the midlatitudes of the Northern Hemisphere (Swann et al. 2012). On the other hand, irrigation artificially fetches water from groundwater storage, which affects the surface soil conditions and atmospheric stability (Lo and Famiglietti 2013). In addition to the surface temperature gradient, land–sea temperature contrast changes could also influence large-scale circulation. For example, Jin and Wang (2017) pointed out that the increased precipitation over the Indian peninsula is due to a stronger Indian monsoon circulation associated with the land–sea temperature contrast changes over the past 15 years. Hohenegger and Stevens (2018) proposed that the circulation might penetrate inland regions and construct a stronger circulation due to the enhancement of sensible heat flux gradient. Therefore, the meridional temperature gradient and the land–sea temperature contrast, which result from the changes in soil moisture or land surface conditions, might alter the intensity and position of the Hadley and monsoon circulations.

The impacts of surface latent heat flux on the atmosphere and their nonlinear interactions have been considered (Laguë et al. 2019; Shukla and Mintz 1982); however, the involvement of atmospheric energy transport (Hill et al. 2015; Hwang and Frierson 2010; Hwang et al. 2013; Kang and Held 2012; Kang et al. 2018) has not been discussed thoroughly in the perspective of changes in the water table dynamics. While previous studies have shown the effects of SST and CO_2 forcings (Held and Soden 2006; Seager et al. 2003) and land-use changes (Swann et al. 2012) on the atmospheric energy transport, this study further focuses on the role of the soil wetness conditions. This study investigates the global-scale responses of atmospheric energy transport between the hemispheres through model experiments with different water table depths and analyses, particularly for the Hadley and South Asian monsoon circulations. We thus conduct idealized experiments with globally fixed shallow and deep water table depths at 1 m and 8 m, respectively, via the Community Earth System Model (CESM) Atmospheric Model Intercomparison Project (AMIP)-type simulations, which use prescribed sea surface temperatures and sea ice fractions from 1949 to 2008.

2. Model simulations and methodology

a. CESM experiments

The SST pattern usually plays a crucial role in affecting the thermodynamic and dynamic components of the rainfall changes over the tropics (Grose et al. 2014; Long et al. 2016; Ma and Xie 2013). When the observational SST is utilized to drive the climate models, the uncertainties of precipitation projection over the tropics can be reduced in the model simulations owing to the tight coupling between the atmosphere and ocean (Long et al. 2016). Thus, in this study, we conduct AMIP-type simulations to investigate the changes in tropical and South Asian monsoon circulations and the global energy transport under different fixed water table depths over landmasses. The atmospheric model [Community Atmosphere Model (CAM); Neale et al. 2012] of CESM and its land component [Community Land Model (CLM); Oleson et al. 2010; Lawrence et al. 2011] are run at $1.9^\circ \times 2.5^\circ$ global resolution, with 30 vertical layers for the CAM. The simulations use the prescribed SST and sea ice fractions from 1949 to 2008.

Figure 1a shows the schematic plot of the soil layer in CLM and the experiment settings. Soil depth in CLM is 3.8 m, with 10 soil hydrologic active layers. Vertical soil water fluxes are calculated using a revised numerical solution of the one-dimensional Richards equation (Zeng and Decker 2009). Two coupled experiments conducted with CAM version 5 and CLM version 4 run in satellite phenology mode are presented here: a shallow water table run (D1) and a deep water table run (D8). In the D1 and D8 simulations, we add (subtract) water into (from) the saturated zones to the fixed water table at 1 and 8 m everywhere over landmasses, as illustrated in Fig. 1a. The D1 experiment can represent wet conditions, while the D8 experiment is for dry conditions. The dry experiment is very close to the simulations of free gravity drainage. The vertical soil water exchanges between the unsaturated and saturated zones through the exchange of soil water flux and capillary rise at the bottom of the unsaturated soil column, but without horizontal soil water fluxes between neighboring grid cells. The soil moisture above the water table depth is active and can interact with other soil layers vertically. Additionally, Figs. 1b and 1c demonstrate the climatology of water table depth and soil moisture in the top 10 cm for the control experiment, with active water table depth. The results show that most subtropics have deep water tables and low soil moisture, such as California, the Sahara Desert, and

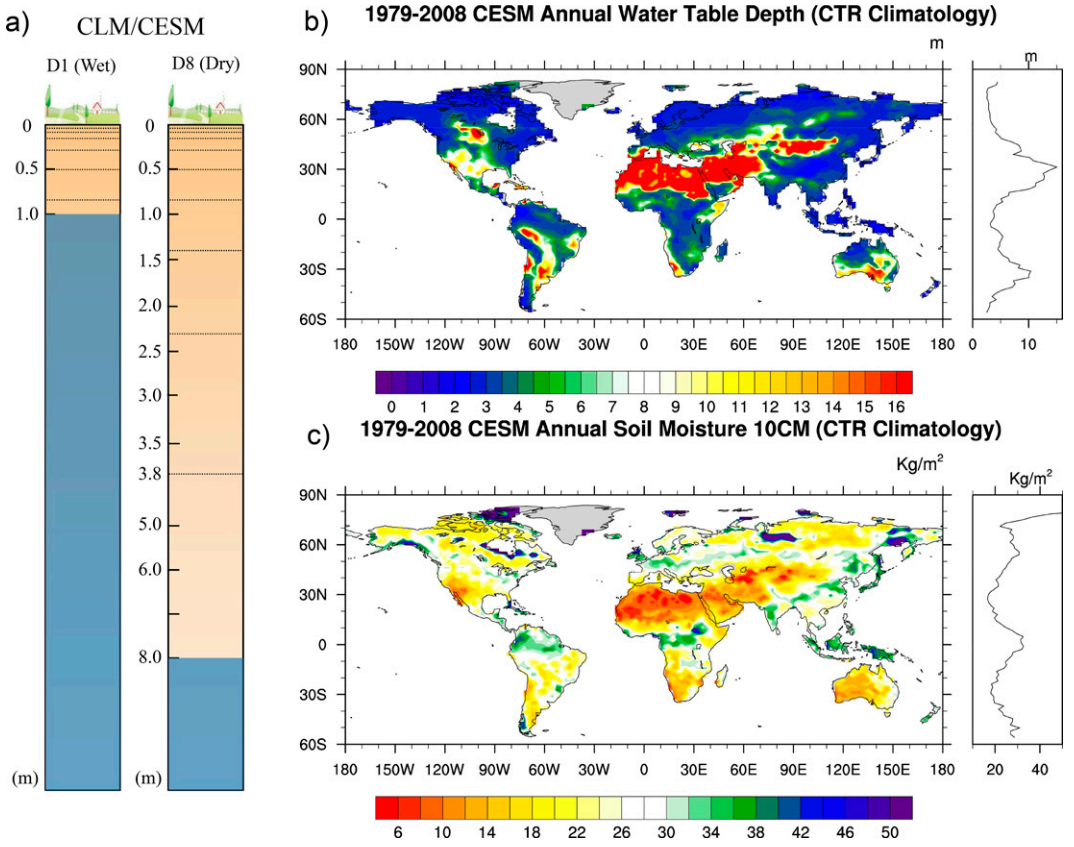

FIG. 1. (a) The schematic plot of the soil layer in CLM and the experiment setting for the fixed shallow water table (D1) and deep water table runs (D8). (b) The climatology of water table depth and (c) the climatology of soil moisture in the top 10 cm from 1979 to 2008 for the control run, with active water table depth, in CESM AMIP-type simulation.

the Middle East; on the contrary, the tropics, monsoon regions, and mid- to high latitudes reveal relatively shallower water tables and high soil moisture (Figs. 1b,c). In the wet experiments, we can expect that the vertical upward water flux (capillary rise) from the groundwater aquifer into the unsaturated soil layers is significantly increased and then causes higher soil moisture. In the meantime, the evaporation into the atmosphere increased much more in the arid regions but increased less in the humid regions when comparing to the dry experiment. As a result, the impacts of water table depth on atmospheric energy responses can be identified from the two experiments' differences (anomalies). We also conducted an ensemble of 10 members with different initial conditions at 0000 UTC (coordinated universal time) on 1 January from 1949 to 1958 for D1 and D8. The simulation processes data from 1959 to 2008 and we only analyze the results from 1979 to 2008, while the 1959–78 period is treated as a spinup period. In this study, although such experiments are idealized simulations, we make the land continent wetter to approach the aquaplanet simulations (zonally symmetric planet with less land–sea contrast) and investigate how such soil moisture variations affect the atmospheric energy transports.

b. *Moist static energy analysis*

In the view of global energy conservation, moist static energy (MSE) is utilized as follows:

$$h = C_p T + \Phi + L_v q, \tag{1}$$

where h is moist static energy (MSE), T is absolute air temperature, q is specific humidity, Φ is geopotential, C_p is the specific heat at constant pressure (1004.0 J kg^{-1} K^{-1}), and L_v is the latent heat of vaporization (2.5×10^6 J kg^{-1}). Equation (1) includes specific heat, geopotential energy, and latent heat energy. The sum of the first two terms indicates dry static energy (DSE), exclusive of latent energy (LE). Equation (2) is further used to describe the various terms of total atmospheric energy transport (left-hand side), which followed Wu et al. (2010), Hill et al. (2015) and Kay et al. (2012):

$$[\overline{vh}] = [\overline{[v][h]}] + [\overline{v^* h^*}] + [\overline{v'h'}], \tag{2}$$

where the overbar $\overline{(\,)}$ denotes annual mean or monthly mean from 1979 to 2008, the prime $(\,)'$ denotes the anomaly from the annual mean or monthly mean, square brackets [ ] represent the zonal mean, an asterisk $(\,)^*$ equals the zonal mean

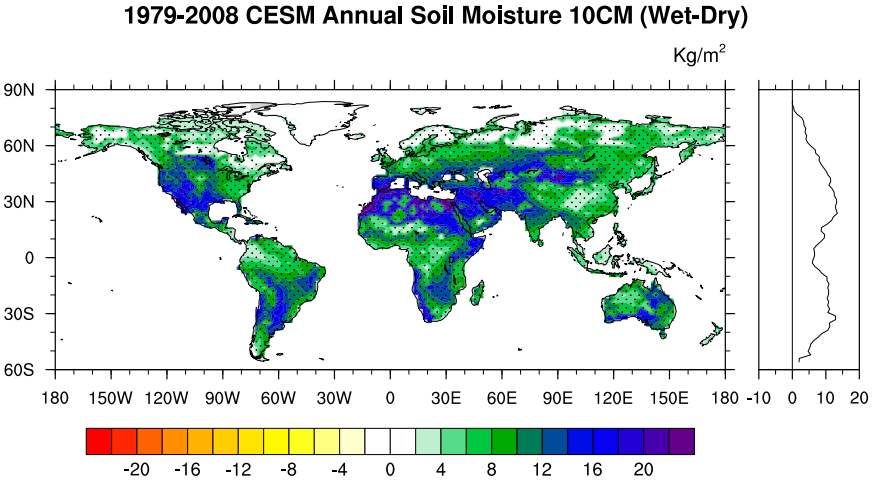

FIG. 2. The difference of the soil moisture of the top 10 cm in spatial climatology and the zonal mean between the wet and dry experiments in CESM AMIP-type ensemble simulations. The stippling indicates regions where the ensemble means deviate significantly from the simulated 1979–2008 period (by at least two standard deviations of internal variability) and where all of the members agree on the sign of the change of the ensemble mean.

subtracted from the total value, h means the moist static energy, and v indicates the meridional wind. The first term ($[[\overline{v}][\overline{h}]]$), the zonally mean part, on the right-hand side of Eq. (2) gives the contribution from mean meridional circulation (MMC). The second term ($[\overline{v^*h^*}]$), the nonzonal mean part, gives the contribution from stationary eddies, and the third term ($[\overline{v'h'}]$) gives the one from transient eddies mostly attributed to the midlatitudes (Hill et al. 2015; Trenberth and Stepaniak 2003). The transient eddies are calculated from the difference between total and quasi-stationary eddies, directly from the monthly dataset. Due to the numerical errors when applying the integration on the terrain, we used the source and sink of net atmospheric energy flux to obtain the MSE and LE. Kay et al. (2012) also proposed such residual methodology regarding the calculation of the northward energy transports. Hence, the MSE in the left term of Eq. (2) is calculated from the net energy flux into the atmospheric column. LE is from the precipitation minus surface latent heat flux. The difference between MSE and LE is DSE. On the other hand, the right-hand side terms are calculated from the monthly divergence of MSE and DSE, but the difference (MSE minus DSE) is LE. Note that each term of energy transport is vertically integrated from the surface to the top of the model, and there are only monthly model outputs used.

Furthermore, to figure out the primary contributions to the difference of MSE transport through the tropical circulation between wet and dry experiments, we decompose the MSE of MMC into the thermodynamic (MSE, DSE, and LE) and dynamic (circulation intensity) components. The meridional wind and MSE in the wet experiment can be described as

$$v_{\text{wet}} = \delta v + v_{\text{dry}},$$

$$h_{\text{wet}} = \delta h + h_{\text{dry}},$$

where δ is the difference between wet and dry experiments; thus, the MSE of MMC transport ($[[\overline{v}][\overline{h}]]$) for wet experiments can be represented as follows:

$$[[\overline{v_{\text{wet}}}][\overline{h_{\text{wet}}}]] = [[\overline{v_{\text{dry}}}][\overline{\delta h}]] + [[\overline{\delta v}][\overline{h_{\text{dry}}}]] + [[\overline{\delta v}][\overline{\delta h}]] + [[\overline{v_{\text{dry}}}][\overline{h_{\text{dry}}}]]. \quad (3)$$

The first term of the right-hand side in Eq. (3) is the contribution from the changes of MSE itself, which is denoted as the thermodynamic component related to the MSE changes. The second term is attributed to the changes in meridional wind, which indicates the dynamic component associated with the changes in circulation intensity. The third term is the nonlinear term. As shown in Eq. (1), the MSE includes DSE and LE parts; thus, the equation is still conserved when the DSE and LE replace the MSE in Eqs. (2) and (3).

3. Results

a. Surface flux changes

Figures 2–4 demonstrate the climatological difference of soil moisture in the top 10 cm, surface latent heat flux, and 2-m temperature between the D1 (wet soil condition) and D8 (dry soil condition) simulations. Figure 2 illustrates more increased soil moisture in the top 10 cm over subtropical arid regions, such as Australia, western North America, South America, North Africa, and central Asia, but less increased soil moisture over the deep tropics in the wet experiments. The regions with robustly increased soil moisture are consistent with climatic deep water table depths and dry soil moisture, as shown in Figs. 1b and 1c. Over these regions, because of drier climate conditions, there is more vertical water flux into the unsaturated soil layers from groundwater via capillary fluxes in the wet experiments; then, the excess water

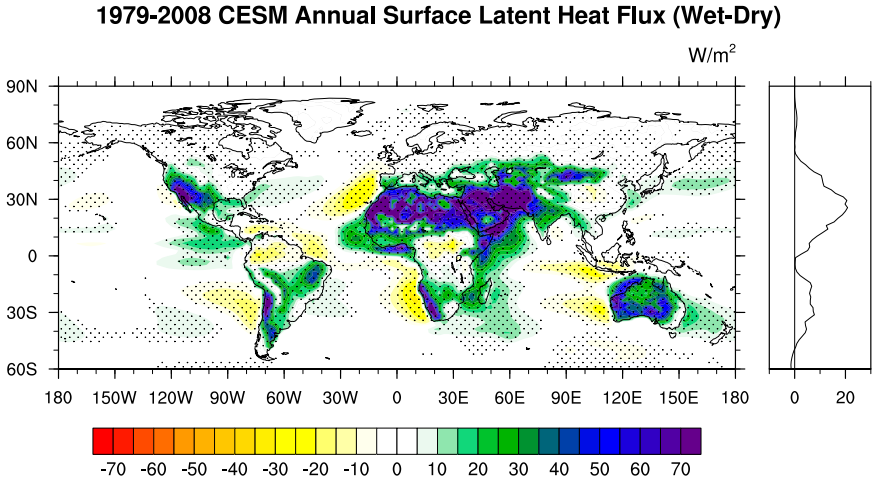

FIG. 3. As in Fig. 2, but for the surface latent heat flux.

evaporates into the atmosphere through the land–atmosphere interactions. In contrast, the deep tropics and mid- to high latitudes have a climatic shallow water table depth and wet soil moisture generally, and thus less vertical water flux into the unsaturated soil layers. Consequently, the 10-cm soil moisture over the subtropical arid climatic regions increases much more than those over the tropics and mid- to high latitudes; more importantly, notable quantities of water vapor are transported into the atmosphere by land evapotranspiration in the wet experiments (Figs. 2 and 3). Such increased surface latent heat flux could cause surface cooling, particularly in the low- to midlatitude land areas (Fig. 4). Note that all 10 members agree on the sign of change in the ensemble mean and the variation of the 10 members is much smaller than the ensemble-mean difference between the wet and dry experiments.

In fact, some ocean areas demonstrate surface latent heat flux changes in spite of conducting the AMIP-type simulations in this study (Fig. 3). The most likely reason is that the wet experiments cause more surface latent heat fluxes over land, leading to land surface cooling and different temperature contrasts between land and ocean. This then results in changes of local and large-scale circulation as well as the net radiation. On the other hand, in the tropics the decreased surface latent heat flux over northern Congo and northern South America is partly associated with more cloud cover (Fig. S1 in the online supplemental material), leading to less net surface shortwave radiation (Fig. S2). Conversely, increased surface latent heat flux in the desert regions and southwest of North America is in relation to robustly increased soil moisture from the groundwater. In the mid- to high latitudes, there are fewer changes because of the climatic shallow water table and wet soil moisture conditions. It is worth noting that the decreased surface albedo in association with the wet soils in the tropics and subtropics results in more surface shortwave radiation absorption; however, the surface cooling from the latent heat flux is much stronger than the effect of decreased surface albedo, which in sum causes the reduced surface temperature (Fig. S3).

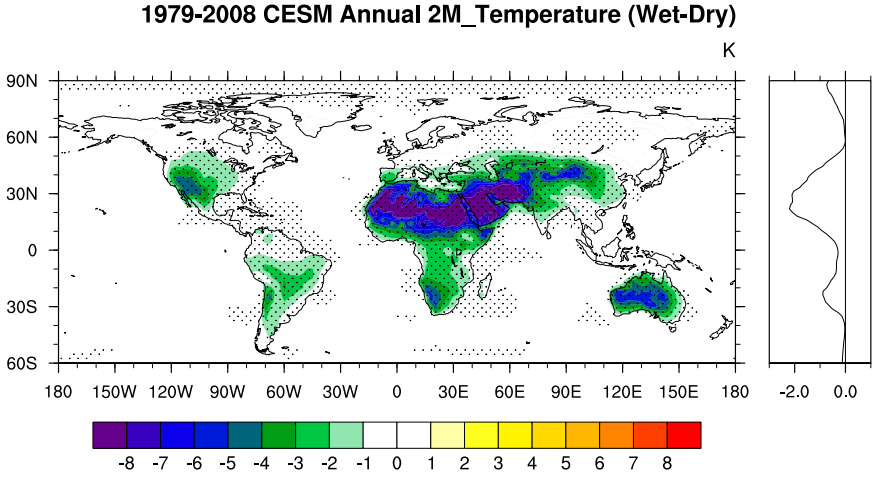

FIG. 4. As in Fig. 2, but for the 2-m air temperature.

The zonal mean differences in surface latent heat flux and 2-m temperature (right panels of Figs. 3 and 4) show that the corresponding maximum and minimum anomalies occur near 30°N and 30°S. In contrast, 2-m temperature around the equator does not change significantly (Fig. 4), combined with the decreased 2-m temperature between wet and dry experiments near 30°N and 30°S that corresponds to an enhancement of the meridional temperature gradient under wet soil conditions. Moreover, the surface latent heat flux and 2-m temperature changes are insignificant in the humid parts of the boreal areas and the mid- to high latitudes, north of 60°N. That is probably because the climate is wet enough in the model to prevent significant water stress onto evapotranspiration (i.e., the energy-limited environment).

b. *Total moist static energy transports*

Figures 5a and 5b show that the climatology of dry experiments and the difference between wet and dry experiments in total MSE, DSE, and LE transports with the spreads of 10 members. The climatology of the dry experiments demonstrates that the MSE is transported poleward in both hemispheres; additionally, the large-scale tropical circulation would tend to transport DSE poleward and LE equatorward, as shown in Fig. 5a. The spread of 10 members in the climatology of dry experiments in total MSE, DSE, and LE transports is very small. Conceptually, the DSE poleward transport is moved by the upper branch of tropical circulation and subsidence on the subtropical surface. The subtropical surface has more solar energy input due to relatively clear skies. Hence, relatively more water vapor from excess evaporation feeds into the atmosphere and supplies the equatorward flow of latent energy into the upward branch of the Hadley circulation in the tropics (Trenberth and Stepaniak 2003).

Because much more surface latent heat flux compensates the noticeably decreased net surface longwave radiation and sensible heat flux, the total MSE in the Northern Hemisphere between wet and dry experiments is nearly neutral. On the contrary, the Southern Hemisphere, near 20° to 40°S, does not show robustly declined net surface longwave radiation and sensible heat flux, but has slightly increased surface latent heat flux and net radiation on the top of model (Fig. S4). Therefore, the total MSE is slightly increased in the midlatitudes of the Southern Hemisphere in the wet experiments (Fig. 5b). The enhancement of DSE poleward and LE equatorward transports is associated with the redistribution of total MSE and the intensity of tropical circulation, instead of different net energy flux into the atmospheric column. Figure 5b represents the enhancements of poleward transport of total DSE with extreme changes at around 8°N and slightly equatorward transport of total LE over the Northern Hemisphere subtropics. The changes in surface latent heat fluxes and surface temperature are rather small in the Southern Hemisphere because of fewer arid lands. As a consequence, the DSE and LE changes in the southern branch of tropical circulation are weaker than those of the northern branch. Such enhancements in the total DSE and LE might be related to both the stronger and equatorward shift in the tropical circulation of the northern branch. Note that our investigated regions, the tropical and South Asian monsoon regions, coincide with the location of the maximum changes in the total DSE and LE, around 40°S–40°N.

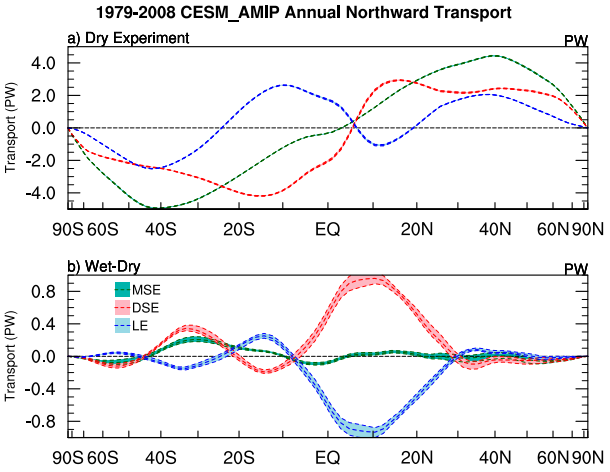

FIG. 5. (a) The climatology of the dry experiment and (b) annual mean difference between the wet and dry experiments in total MSE, DSE, and LE transports in CESM AMIP-type ensemble simulations. Positive (negative) values indicate northward (southward) transport. The dashed lines indicate the ensemble mean, and the shadings are the range between maximum and minimum values in ensemble members.

c. *Responses of circulation to the MMC and SE transports*

Following Eq. (2), the zonal mean of energy transport is decomposed into its main transport components, the mean meridional circulation (MMC) and the stationary eddies (SE). Figures 6a and 6b confirm that total DSE and LE have much stronger anomalies in the Northern Hemisphere tropics than in the Southern Hemisphere. Figures 6a–d show that the enhancements in DSE and LE transports of MMC are very similar to those in DSE and LE of total atmospheric energy transport, indicating that most changes in atmospheric energy transport are through the changes of MMC. Moreover, a noticeably monthly mean difference in DSE and LE of MMC exists from January to June in the Northern Hemisphere and from August to January in the Southern Hemisphere. To put it another way, the atmospheric energy transport is also adjusted in accordance with the different water table depths.

We next turn to investigate what the primary contribution to such changes of MMC transport is. The MMC transport is then decomposed to the thermodynamic (related to the changes of MSE, DSE, and LE themselves) and dynamic components (associated with the general circulation intensity changes), as shown in Fig. 7. Regarding the MSE of MMC, Fig. 7a illustrates that the differences between wet and dry experiments are tiny, particularly in the Northern Hemisphere. Figures 7b and 7c demonstrate the apparent complementarity for DSE and LE of MMC; meanwhile, primary contributions of such changes are attributed to the dynamic component

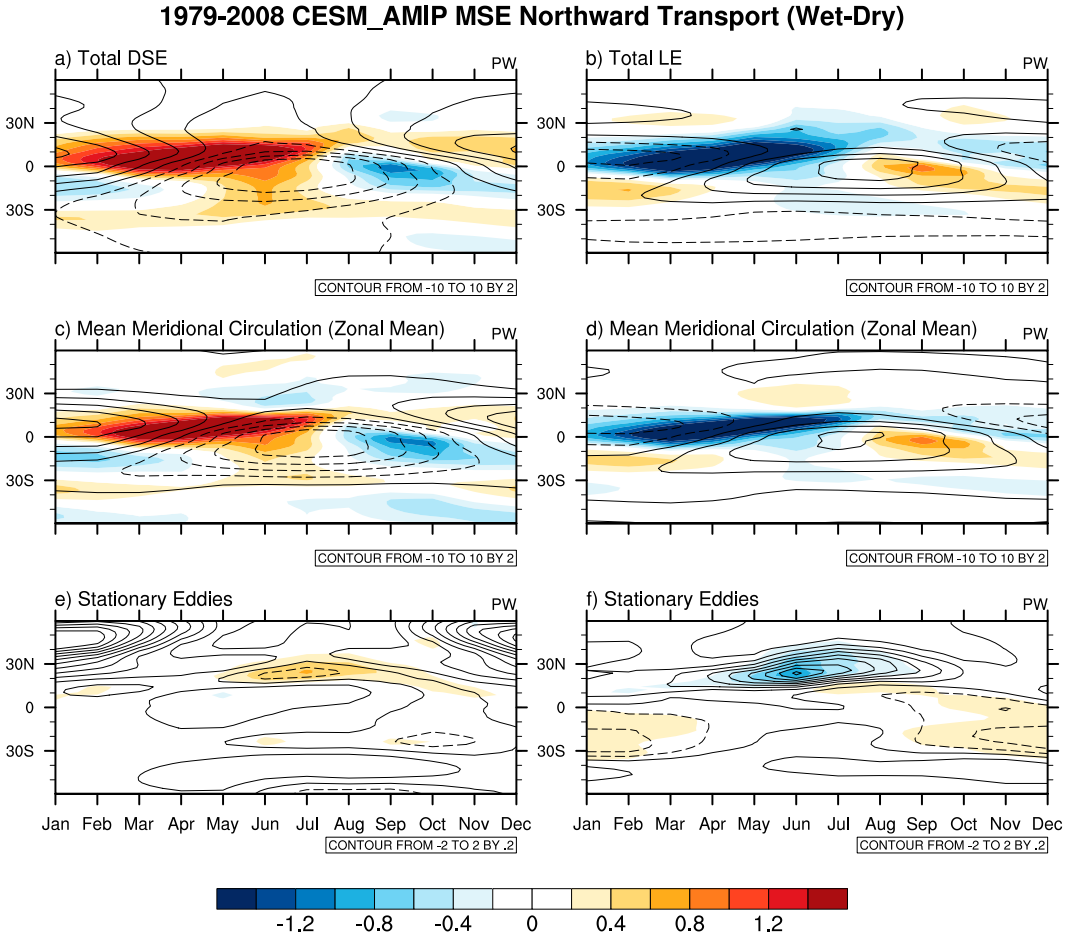

FIG. 6. The monthly mean difference between wet and dry experiments (shading) and climatology of the dry experiment (contours) in (a) total DSE, (b) total LE, (c) mean meridional circulation of DSE, (d) mean meridional circulation of LE, (e) stationary eddies of DSE, and (f) stationary eddies of LE in CESM AMIP-type ensemble simulations.

(red dashed lines), particularly over the tropics. The thermodynamic component (blue dashed lines) is much smaller than the dynamic part, indicating that the enhancing Hadley circulation invokes the changes in tropical energy transport in DSE and LE of MMC. In addition, the dynamic component has its extrema at around 8°N, consistent with the changes in DSE and LE transports, which also indicate a partly equatorward shift of Hadley circulation in the wet experiments.

The climatology and its difference in the zonal mean mass streamfunction also demonstrate a stronger Hadley circulation with slightly equatorward shifting and narrowing of the wet soil condition (Fig. 8; see also Fig. S5). The results are consistent with the changes of LE and DSE transports in Fig. 5b, where the strongest signals occur at around 8°N and slightly cross the equator. The 2-m temperature in 30°N is lower about 2 K in the wet experiments than in the dry experiments, but nearly the same at the equator (Table 1). As a result, the meridional temperature gradient over the tropics (the difference between the equator and 30°N) is more robust in the wet experiments (7.24 K) compared to that of the dry experiments (5.45 K). Relative to the dry soil experiments, the Hadley circulation of the wet soil experiments becomes stronger, slightly narrower, and shifted equatorward over the Northern Hemisphere because of the stronger meridional temperature gradient (Seo et al. 2014). Hwang et al. (2013) proposed that the cooling in the Northern Hemisphere owing to the sulfate aerosol could induce the southward shift of the Hadley circulation, tropical precipitation, and energy transports across the equator attributed to the temperature asymmetry changes between two hemispheres.

d. South Asian monsoon circulation

Under our experiments design, because less land–sea thermal contrast reduces the zonal asymmetry, the nonzonal (SE) energy transport reduces but the zonal mean (MMC) enhances, as shown in Figs. 6c–f. The climatology of stationary eddies shows equatorward DSE and poleward LE transports with robust reductions of DSE and LE transports near 30°N in July and August (Figs. 6e,f). In terms of the spatial divergence of DSE and LE in July (Fig. S6), the maximum reduction of equatorward DSE and poleward LE transports is over the western Indian peninsula and East Africa. The anomalous

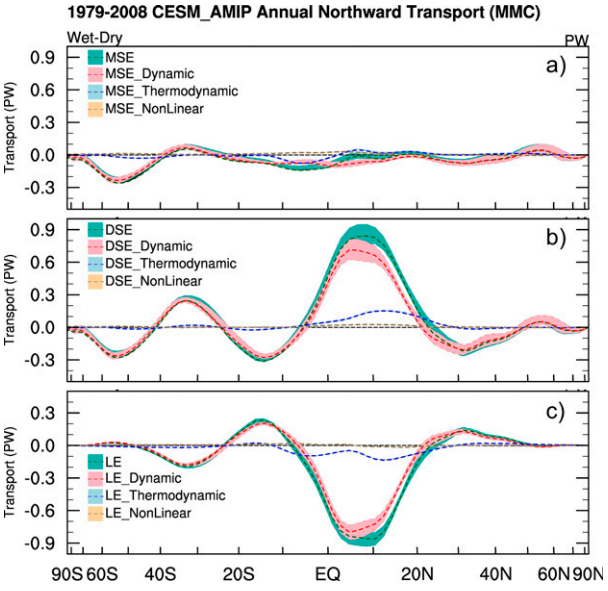

FIG. 7. The annual mean difference between the wet and dry experiments in decomposed the mean meridional circulation for (a) MSE, (b) DSE, and (c) LE transports in CESM AMIP-type ensemble simulations. Positive (negative) values indicate northward (southward) transport. The dashed lines indicate the ensemble mean, and the shadings are the range between maximum and minimum values in ensemble members.

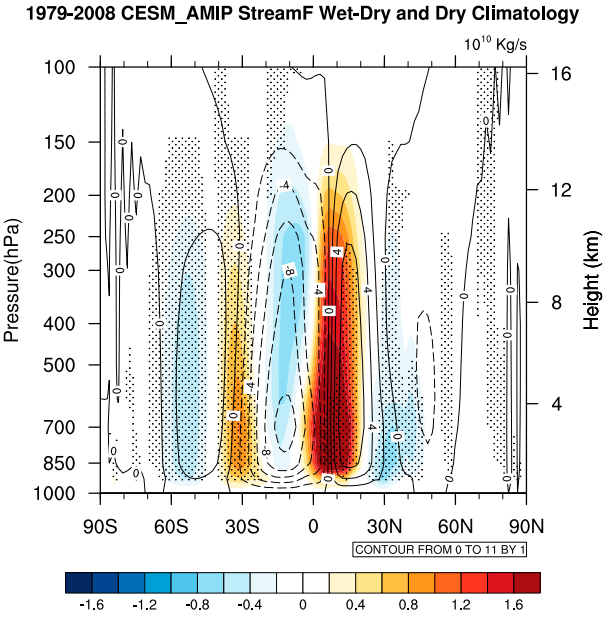

FIG. 8. Zonal-mean mass streamfunction of climatology difference (shading) between the wet and dry experiments and climatology in the dry experiment (contour) in CESM AMIP-type simulations. The stippling indicates regions where the ensemble means deviate significantly from the simulated 1979–2008 period (by at least two standard deviations of internal variability) and where all of the members agree on the sign of the change of ensemble mean. The positive values of the streamfunction indicate clockwise zonal circulation.

DSE and LE of SE shown in Figs. 6e and 6f are likely associated with the mature South Asian monsoon circulation weakening. To further investigate the changes in South Asian monsoon circulation, we used the Webster-Yang Monsoon Index (WYMI) (Webster and Yang 1992), which calculates the averaged difference between U at 850 and 200 hPa (0°–20°N, 40°–110°E), and represented the fixed geographical structure of the South Asian monsoon circulation at 850 and 200 hPa. Figure 9 demonstrates the obviously weakened monsoon index in the premonsoon period from April to June in the wet experiments. Because of the consistent months between WYMI and MMC changes, such robustly weakening WYMI might be associated with enhancing MMC energy transport, as shown in Figs. 6c and 6d. On the other hand, the WYMI in the mature phase of the South Asian monsoon (July and August) slightly weakened in the wet experiments, possibly in relation to the reduction of poleward (equatorward) LE (DSE) transport in SE.

Walker and Bordoni (2016) show that the wind transition at 200 and 850 hPa can be linked to the monsoon circulation and onset timing. Figures S7 and S8 demonstrate the wind transition at 850 and 200 hPa from April to September in the wet and dry experiments, respectively. In the wet experiments, the cross-equatorial flow from the Southern Hemisphere is near the equator in May but penetrates the Indian peninsula in the dry experiment. In June, the monsoon circulation of the wet experiment is located over farther southern India than that of the dry experiment, as shown in Fig. S7. Additionally, regarding the circulation at 200 hPa, the South Asian high with anticyclonic circulation is over southern India in May in the wet experiment, but it is over northeastern India in the dry experiment (Fig. S8). In July and August, circulations at 850 and 200 hPa in the wet and dry experiments are similar, but slightly weaker in the wet experiment. In addition, Fig. S9 demonstrates that the maximum U-wind at 850 hPa from May to August appears more southward in the wet experiment (D1.0) compared to that of the dry experiment (D8.0). The findings of anomalous wind transitions in the wet and dry experiments are consistent with the differences of the fixed geographical monsoon index, which is the WYMI. In accordance with the findings of wind transition, the smaller WYMI in the wet experiments is most likely attributable to the southward shifts of the South Asian monsoon circulation, rather than its intensity changes. Consequently, the Hadley and southward shifts of the South Asian monsoon circulations in the wet experiments would possibly interact with each

TABLE 1. The averages of 2-m temperature at the equator and 30°N, and their differences in the wet and dry experiments. The ensemble mean ± one standard deviation across the distribution of 10 ensemble members are shown.

Expt	Equator	30°N	Difference
Wet	298.68 ± 0.004	291.44 ± 0.018	7.24 ± 0.017
Dry	298.97 ± 0.004	293.52 ± 0.015	5.45 ± 0.016

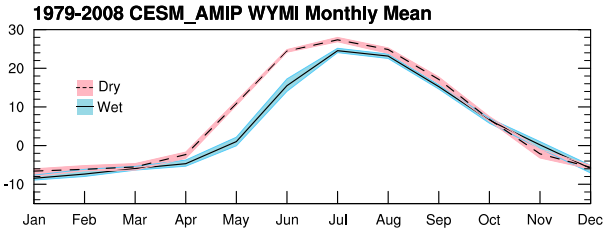

FIG. 9. The seasonal cycle of the WYMI of the wet and the dry experiments in CESM AMIP-type simulations. The black lines indicate the ensemble mean, and the shadings are the range between maximum and minimum values in ensemble members.

other (Geen et al. 2020; Hu et al. 2018). As a whole, the South Asian monsoon circulation shifts robustly southward in the premonsoon season, and is slightly weakened in July and August. Moreover, South Asia also has a delayed monsoon onset in the wet experiment due to the wet soil conditions with longer persistence compared to the dry conditions.

Figure 10a represents the reduction of precipitation over the South Asian monsoon regions and enhanced precipitation in tropics in wet experiments from May to June, which might be related to the combined effects of the southward shift of monsoon circulation and the equatorward shift of the stronger Hadley circulation in the premonsoon season. The zonal mean, shown in the right panel of Fig. 10a, demonstrates the decreased precipitation near 15°N, which is related to the reduction of precipitation over the South Asian monsoon regions. We further evaluate the averages of 2-m temperature over the subcontinent and tropical Indian Ocean in wet and dry experiments during the premonsoon season (May and June), following Jin and Wang (2017). They suggested that the temperature contrast between the subcontinent and tropical Indian Ocean is consistent with the monsoonal precipitation. Table 2 presents that the land–sea temperature contrast in the dry experiments (0.81 K) is significantly larger than in the wet experiments (0.56 K) with 99.9% confidence level. As a consequence, this means that such weaker land–sea temperature contrast changes altered by different water table depths in the wet experiments could cause the southward shift of monsoonal circulation and the precipitation reduction over South Asia, and further cause the delayed South Asian monsoon onset (Fig. 10a).

In Fig. 10b, there is significantly increased precipitation over the tropical Indian Ocean, tropical Atlantic Ocean, and

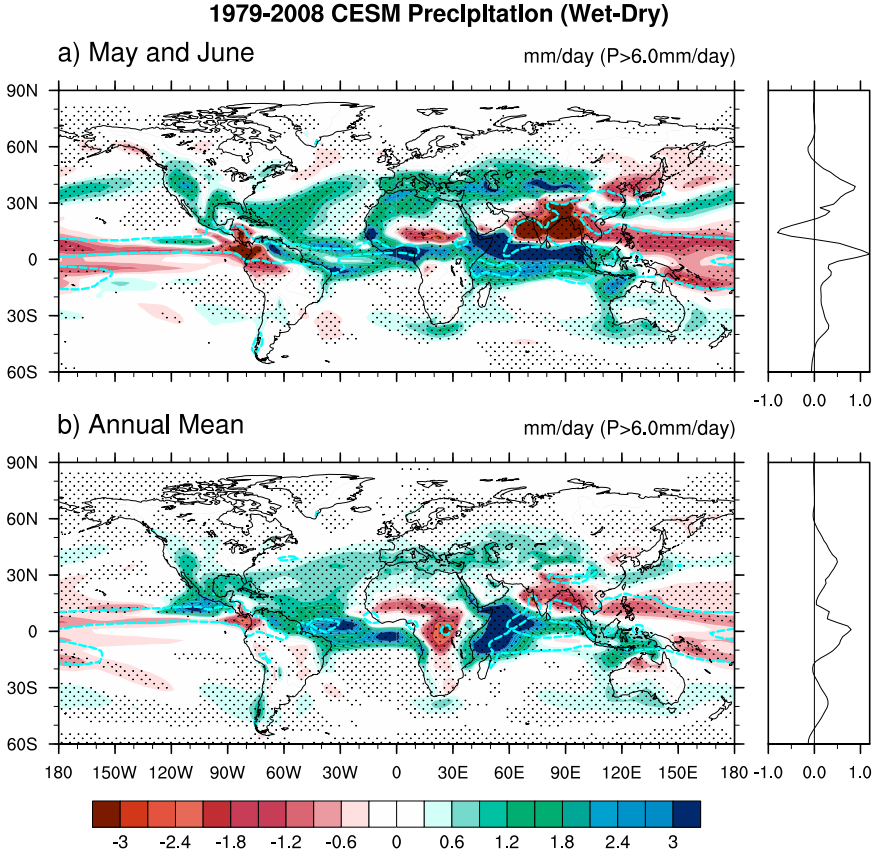

FIG. 10. As in Fig. 2, but for (a) the precipitation of the climatology difference in May and June and (b) the precipitation of the annual climatology difference. The cyan dashed lines indicate the regions with precipitation climatology greater than 6 mm day^{-1} in the ensemble mean of dry experiments.

TABLE 2. The averages in the Indian subcontinent (10°–30°N, 70°–90°E) and tropical Indian Ocean (10°S–25°N, 40°–100°E) boxes during May–June in the wet and dry experiments. The ensemble mean ± one standard deviation across the distribution of 10 ensemble members are shown.

Expt	Indian subcontinent	Tropical Indian Ocean	Difference
Wet	300.79 ± 0.062	300.23 ± 0.014	0.56 ± 0.052
Dry	302.46 ± 0.068	301.65 ± 0.018	0.81 ± 0.053

western Mexico. In contrast, there is decreased precipitation over the Amazon rain forest, Congo rain forest, South Asian monsoon region, and ITCZ in the Pacific Ocean. Such inhomogeneous changes might be in relation to the Hadley, monsoonal, and local circulation changes. Although the annual zonal mean of precipitation is increased over the equator, the tropical precipitation is reduced over the upward motion regions (cyan contour) due to the anomalous downward motion (Fig. 10b). In the meantime, there is enhanced precipitation over the Atlantic Ocean and the western Indian Ocean. The result indicates that the stronger Hadley circulation of the global zonal mean in the wet experiments is most likely attributed to the enhancement of local Hadley circulation over the Indian and Atlantic Oceans.

4. Discussion

a. *Experimental design and AMIP-type simulations*

This study analyzes the difference between experiments with a fixed water table of 1 and 8 m to obtain significant results. Although the experimental design might not be realistic, we can more clearly investigate the impacts of different water tables on atmospheric circulations through such idealized simulations. As shown in Figs. 2–4, despite the same difference of the water table depths globally, because of the original climatic conditions the soil moisture and surface latent heat flux do not reveal homogenous increases, with much more over the subtropical arid regions and less over the humid regions. In addition, Figs. S10 and S11 show the climatological difference of surface latent heat flux and precipitation between control and dry (8 m) experiments. The results demonstrate that the D8 experiments dry more areas (outside the arid regions) than the control experiments do, such as monsoon regions, the Amazon, and the midlatitudes. The changes in surface latent heat flux and precipitation are much smaller between control and dry experiments than those between wet and dry, roughly one-tenth the magnitude. Thus, we use a dry experiment instead of the control simulation in this study to have the maximum difference. Furthermore, the simulated water table depth varies spatially in the control experiment, as shown in Fig. 1b, which provides another dimension in such comparisons. More importantly, in this study, the robust moistening in subtropical arid regions is responsible for the Hadley and monsoon circulation changes. When the water tables change, the arid regions are crucial and sensitive to the large-scale circulation, even to the monsoon circulation's position in the premonsoon season, because of mostly water-limited climates in the arid regions (Fraedrich et al. 2014; McVicar et al. 2012). Consequently, such changes are primarily attributed to the contribution of the arid regions in wet simulations rather than dry simulations.

Regarding the AMIP-type simulations, Laguë et al. (2019) explored the effect of changes in terrestrial evaporation in CESM with varied SSTs. Hill et al. (2015) conducted the model simulation based on the prescribed SST and investigated the aerosol forcing response by calculating energy transport. In short, in this study, the MSE transport and atmospheric circulations are primarily driven by the prescribed SSTs. Nevertheless, the terrestrial forcing can still cause a significant impact on the atmospheric circulation via the land–sea temperature contrast, then resulting in a robust enhancement of tropical energy transport. In other words, the changes in the terrestrial evaporation altered by the fixed water table depth might be modulated by SSTs. To figure out the signal from different water table depths and avoid feedbacks from the ocean dynamics, we use the fixed SSTs experiments. Undoubtedly, the nonlinear interactions in the Earth system model might play some modulation roles on the impacts of altering water table depth; hence, including the ocean dynamic or SST variations in the model experiments can further modulate the atmospheric meridional energy transport, which will be useful follow-up work.

b. *Moist static energy transports*

The wet experiments of the study reduce the land–sea temperature contrast and enhance zonal symmetry. The stationary eddy energy reduces, but the mean meridional circulation enhances, coinciding with the southward shifts of South Asian monsoon circulation and stronger Hadley circulation. Such energy transport characteristics are similar to aquaplanet simulations, with enhanced MMC and reduced SE. Additionally, in the wet experiments, the precipitation from the South Asian monsoon circulation in the premonsoon season might become part of Hadley circulations owing to its southward shift. From an energetic point of view, the energy transport in the weakened premonsoon circulation might be correlated with the changes in MMC energy transport.

The model results show that the maximum and minimum peaks of atmospheric energy transport changes in total DSE and LE are approximately +1.0 and −1.0 PW, respectively, in the tropical Northern Hemisphere (Fig. 5b). Seager et al. (2003) demonstrated that El Niño events with warmer tropical SST have stronger Hadley circulation compared to that in the La Niña events. In analysis from the ERA-Interim dataset (Dee et al. 2011), the differences of the total DSE and LE climatology in the tropics between El Niño and La Niña events (averaged from July of the developing year to June of the following year) are approximately +0.6 and −0.6 PW, respectively. Besides, the total DSE and LE changes from the SRES A1B scenario between the first and the last 20 years of the twenty-first century are approximately −0.2 and +0.2 PW in the tropical Southern Hemisphere, and roughly +0.1 and −0.1 PW in the Northern Hemisphere tropics (Held and Soden 2006). In terms of the monsoon circulation changes, the seasonality

of stationary eddies in LE changes near 30°N during June is roughly −0.6 PW from different water table depth experiments (Fig. 6f), but the difference between El Niño and La Niña events is less than −0.3 PW in the ERA-Interim dataset. In summary, this study raises the importance of land hydrological processes affecting large-scale energy transport, which have a comparable magnitude of atmosphere energy transport to the interannual variabilities and global warming forcing.

5. Conclusions

We use the idealized experiments with globally fixed water tables to explore how the global energy transport responds to the groundwater variations. In the wet conditions associated with shallow water table depths, there are increased surface latent heat flux and robust surface cooling over the subtropical regions, particularly in the subarid and arid areas. Wet soil moisture anomalies induce a stronger meridional temperature gradient, leading to the enhancement of the poleward DSE and equatorward LE transports by the mean meridional circulation over the tropics in the wet experiments. Such changes are mainly contributed by the dynamic component (i.e., stronger Hadley circulation). Moreover, the land–sea temperature contrast in the premonsoon season is decreased in the wet experiments and causes a southward shift of South Asian monsoon circulation, leading to a delayed monsoon onset accompanied by lower precipitation over South Asia. The southward shifts of monsoon circulation in the premonsoon season was confirmed by the monsoon index and wind transition.

Because of the prescribed uniform water table at 1 m below the soil surface, the wet soil condition experiments with extremely humid land conditions globally conducted here show similarities with the aquaplanet simulation. In this study, the simulated change in the zonal mean of surface temperature corresponds to a stronger meridional gradient and a reduced land–sea temperature contrast, favoring stronger Hadley circulation (Chen et al. 2010; Gastineau et al. 2011; Levine and Schneider 2011; Williamson et al. 2013) and southward shifts of monsoon circulations in the premonsoon season (Liang et al. 2005; Yano 1998). Moreover, the response of atmospheric energy transport to the contrasting soil conditions, as simulated by the averages from 10 CESM simulations, seems significant against the responses to interannual SST variability and the anthropogenic CO_2 forcing. This study also demonstrates that land surface conditions can be an essential driver of global atmospheric energy transport.

Acknowledgments. This study was supported by the NSTC grants 111-2628-M-002-003, 104-2923-M-002-002-MY4, 110-2628-M-002-004-MY4, and 110-2111-M-002-012 to National Taiwan University, and by the French Agence Nationale de la Recherche (ANR Grant ANR-14-CE01-0018-01). The ERA-Interim data used during this study are openly available from the ECMWF website https://apps.ecmwf.int/datasets/data/interim-full-daily/levtype=sfc/ as cited in Dee et al. (2011). The numerical model simulations are based on CESM version 1.03 with CAM version 5 and CLM version 4 with prescribed sea surface temperature, accessible from http://www.cesm.ucar.edu/models/cesm1.0/. The zip files of the buildconf folder, the spatial annual mean, and monthly mean datasets with NetCDF format (T2m, precipitation, surface latent heat flux, soil moisture in top 10 cm, and energy transport) in CESM simulations we conducted have been put in the GitHub repository (https://github.com/JeffBlue1125/NTU-Responses_of_Global_Atmospheric_Energy_Transport_in_GCM). Further information needed to replicate the simulations is upon request from the corresponding author, Min-Hui Lo (minhuilo@ntu.edu.tw).

REFERENCES

Adam, O., T. Schneider, and N. Harnik, 2014: Role of changes in mean temperatures versus temperature gradients in the recent widening of the Hadley circulation. *J. Climate*, **27**, 7450–7461, https://doi.org/10.1175/JCLI-D-14-00140.1.

Berg, A., B. Lintner, K. Findell, and A. Giannini, 2017: Soil moisture influence on seasonality and large-scale circulation in simulations of the West African monsoon. *J. Climate*, **30**, 2295–2317, https://doi.org/10.1175/JCLI-D-15-0877.1.

Betts, A. K., and M. A. F. Silva Dias, 2010: Progress in understanding land-surface-atmosphere coupling from LBA research. *J. Adv. Model. Earth Syst.*, **2**, 6, https://doi.org/10.3894/JAMES.2010.2.6.

Chen, C.-C., and Coauthors, 2019: Thermodynamic and dynamic responses to deforestation in the Maritime Continent: A modeling study. *J. Climate*, **32**, 3505–3527, https://doi.org/10.1175/JCLI-D-18-0310.1.

Chen, G., R. A. Plumb, and J. Lu, 2010: Sensitivities of zonal mean atmospheric circulation to SST warming in an aqua-planet model. *Geophys. Res. Lett.*, **37**, L12701, https://doi.org/10.1029/2010GL043473.

Chen, X., and Q. Hu, 2004: Groundwater influences on soil moisture and surface evaporation. *J. Hydrol.*, **297**, 285–300, https://doi.org/10.1016/j.jhydrol.2004.04.019.

Chen, Z., S. E. Grasby, and K. G. Osadetz, 2002: Predicting average annual groundwater levels from climatic variables: An empirical model. *J. Hydrol.*, **260**, 102–117, https://doi.org/10.1016/s0022-1694(01)00606-0.

——, ——, and ——, 2004: Relation between climate variability and groundwater levels in the upper carbonate aquifer, southern Manitoba, Canada. *J. Hydrol.*, **290**, 43–62, https://doi.org/10.1016/j.jhydrol.2003.11.029.

Chou, C., J. D. Neelin, and H. Su, 2001: Ocean–atmosphere–land feedbacks in an idealized monsoon. *Quart. J. Roy. Meteor. Soc.*, **127**, 1869–1891, https://doi.org/10.1002/qj.49712757602.

Cooper, D. M., W. B. Wilkinson, and N. W. Arnell, 1995: The effects of climate changes on aquifer storage and river baseflow. *Hydrol. Sci. J.*, **40**, 615–631, https:/doi.org/10.1080/02626669509491448.

Croley, T. E., and C. L. Luukkonen, 2003: Potential effects of climate change on ground water in Lansing, Michigan. *J. Amer. Water Resour. Assoc.*, **39**, 149–163, https:/doi.org/10.1111/j.1752-1688.2003.tb01568.x.

DeAngelis, A., F. Dominguez, Y. Fan, A. Robock, M. D. Kustu, and D. Robinson, 2010: Evidence of enhanced precipitation due to irrigation over the Great Plains of the United States. *J. Geophys. Res.*, **115**, D15115, https://doi.org/10.1029/2010JD013892.

Dee, D. P., and Coauthors, 2011: The ERA-Interim reanalysis: Configuration and performance of the data assimilation system. *Quart. J. Roy. Meteor. Soc.*, **137**, 553–597, https://doi.org/10.1002/qj.828.

Evans, A., H. Nguyen, B. Timbal, I. Smith, and C. Lucas, 2012: The Hadley circulation in reanalyses: Climatology, variability, and change. *J. Climate*, **26**, 3357–3376, https://doi.org/10.1175/JCLI-D-12-00224.1.

Fraedrich, K., F. Sielmann, D. Cai, L. Zhang, and X. Zhu, 2014: Validation of an ideal rainfall-runoff chain in a GCM environment. *Water Resour. Manage.*, **29**, 313–324, https://doi.org/10.1007/s11269-014-0703-2.

Gastineau, G., L. Li, and H. Le Treut, 2011: Some atmospheric processes governing the large-scale tropical circulation in idealized aquaplanet simulations. *J. Atmos. Sci.*, **68**, 553–575, https://doi.org/10.1175/2010JAS3439.1.

Geen, R., S. Bordoni, D. S. Battisti, and K. Hui, 2020: Monsoons, ITCZs, and the concept of the global monsoon. *Rev. Geophys.*, **58**, e2020RG000700, https://doi.org/10.1029/2020RG000700.

Grose, M. R., J. Bhend, S. Narsey, A. Sen Gupta, and J. R. Brown, 2014: Can we constrain CMIP5 rainfall projections in the tropical Pacific based on surface warming patterns? *J. Climate*, **27**, 9123–9138, https://doi.org/10.1175/JCLI-D-14-00190.1.

Güntner, A., J. Stuck, S. Werth, P. Döll, K. Verzano, and B. Merz, 2007: A global analysis of temporal and spatial variations in continental water storage. *Water Resour. Res.*, **43**, W05416, https://doi.org/10.1029/2006WR005247.

Gutowski, W. J., C. J. Vörösmarty, M. Person, Z. Ötles, B. Fekete, and J. York, 2002: A Coupled Land–Atmosphere Simulation Program (CLASP): Calibration and validation. *J. Geophys. Res.*, **107**, 4283, https://doi.org/10.1029/2001JD000392.

Held, I. M., and B. J. Soden, 2006: Robust responses of the hydrological cycle to global warming. *J. Climate*, **19**, 5686–5699, https://doi.org/10.1175/JCLI3990.1.

Hill, S. A., Y. Ming, and I. M. Held, 2015: Mechanisms of forced tropical meridional energy flux change. *J. Climate*, **28**, 1725–1742, https://doi.org/10.1175/JCLI-D-14-00165.1.

Hirsch, A. L., J. Kala, A. J. Pitman, C. Carouge, J. P. Evans, V. Haverd, and D. Mocko, 2013: Impact of land surface initialization approach on subseasonal forecast skill: A regional analysis in the Southern Hemisphere. *J. Hydrometeor.*, **15**, 300–319, https://doi.org/10.1175/JHM-D-13-05.1.

Hohenegger, C., and B. Stevens, 2018: The role of the permanent wilting point in controlling the spatial distribution of precipitation. *Proc. Natl. Acad. Sci. USA*, **115**, 5692–5697, https://doi.org/10.1073/pnas.1718842115.

Hu, Y., H. Huang, and C. Zhou, 2018: Widening and weakening of the Hadley circulation under global warming. *Sci. Bull.*, **63**, 640–644, https://doi.org/10.1016/j.scib.2018.04.020.

Hwang, Y. T., and D. M. W. Frierson, 2010: Increasing atmospheric poleward energy transport with global warming. *Geophys. Res. Lett.*, **37**, L24807, https://doi.org/10.1029/2010GL045440.

——, ——, and S. M. Kang, 2013: Anthropogenic sulfate aerosol and the southward shift of tropical precipitation in the late 20th century. *Geophys. Res. Lett.*, **40**, 2845–2850, https://doi.org/10.1002/grl.50502.

Jin, Q., and C. Wang, 2017: A revival of Indian summer monsoon rainfall since 2002. *Nat. Climate Change*, **7**, 587–594, https://doi.org/10.1038/nclimate3348.

Kang, S. M., and I. M. Held, 2012: Tropical precipitation, SSTs and the surface energy budget: A zonally symmetric perspective. *Climate Dyn.*, **38**, 1917–1924, https://doi.org/10.1007/s00382-011-1048-7.

——, Y. Shin, and S.-P. Xie, 2018: Extratropical forcing and tropical rainfall distribution: Energetics framework and ocean Ekman advection. *npj Climate Atmos. Sci.*, **1**, 20172, https://doi.org/10.1038/s41612-017-0004-6.

Kay, J. E., M. M. Holland, C. M. Bitz, E. Blanchard-Wrigglesworth, A. Gettelman, A. Conley, and D. Bailey, 2012: The influence of local feedbacks and northward heat transport on the equilibrium Arctic climate response to increased greenhouse gas forcing. *J. Climate*, **25**, 5433–5450, https://doi.org/10.1175/JCLI-D-11-00622.1.

Kim, J. E., and S. Y. Hong, 2007: Impact of soil moisture anomalies on summer rainfall over East Asia: A regional climate model study. *J. Climate*, **20**, 5732–5743, https://doi.org/10.1175/2006JCLI1358.1.

Koster, R. D., and Coauthors, 2010: Contribution of land surface initialization to subseasonal forecast skill: First results from a multi-model experiment. *Geophys. Res. Lett.*, **37**, L02402, https://doi.org/10.1029/2009GL041677.

——, Y. Chang, H. Wang, and S. D. Schubert, 2016: Impacts of local soil moisture anomalies on the atmospheric circulation and on remote surface meteorological fields during boreal summer: A comprehensive analysis over North America. *J. Climate*, **29**, 7345–7364, https://doi.org/10.1175/JCLI-D-16-0192.1.

Laguë, M. M., G. B. Bonan, and A. L. S. Swann, 2019: Separating the impact of individual land surface properties on the terrestrial surface energy budget in both the coupled and uncoupled land–atmosphere system. *J. Climate*, **32**, 5725–5744, https://doi.org/10.1175/JCLI-D-18-0812.1.

Lawrence, D., and K. Vandecar, 2015: Effects of tropical deforestation on climate and agriculture. *Nat. Climate Change*, **5**, 27–36, https://doi.org/10.1038/nclimate2430.

Lawrence, D. M., and Coauthors, 2011: Parameterization improvements and functional and structural advances in version 4 of the Community Land Model. *J. Adv. Model. Earth Syst.*, **3**, M03001, https://doi.org/10.1029/2011MS00045.

Levine, X. J., and T. Schneider, 2011: Response of the Hadley circulation to climate change in an aquaplanet GCM coupled to a simple representation of ocean heat transport. *J. Atmos. Sci.*, **68**, 769–783, https://doi.org/10.1175/2010JAS3553.1.

Liang, X., Z. Xie, and M. Huang, 2003: A new parameterization for surface and groundwater interactions and its impact on water budgets with the variable infiltration capacity (VIC) land surface model. *J. Geophys. Res.*, **108**, 8613, https://doi.org/10.1029/2002JD003090.

——, Y. Liu, and G. Wu, 2005: The role of land–sea distribution in the formation of the Asian summer monsoon. *Geophys. Res. Lett.*, **32**, L03708, https://doi.org/10.1029/2004GL021587.

Lin, Y. H., M. H. Lo, and C. Chou, 2016: Potential negative effects of groundwater dynamics on dry season convection in the Amazon River basin. *Climate Dyn.*, **46**, 1001–1013, https://doi.org/10.1007/s00382-015-2628-8.

Lo, M.-H., and J. S. Famiglietti, 2010: Effect of water table dynamics on land surface hydrologic memory. *J. Geophys. Res.*, **115**, D22118, https://doi.org/10.1029/2010JD014191.

——, and ——, 2011: Precipitation response to land subsurface hydrologic processes in atmospheric general circulation model simulations. *J. Geophys. Res.*, **116**, D05107, https://doi.org/10.1029/2010JD015134.

Lo, M. H., and J. S. Famiglietti, 2013: Irrigation in California's Central Valley strengthens the southwestern U.S. water cycle.

Geophys. Res. Lett., **40**, 301–306, https://doi.org/10.1002/grl.50108.

Long, S.-M., S.-P. Xie, and W. Liu, 2016: Uncertainty in tropical rainfall projections: Atmospheric circulation effect and the ocean coupling. *J. Climate*, **29**, 2671–2687, https://doi.org/10.1175/JCLI-D-15-0601.1.

Lu, J., G. A. Vecchi, and T. Reichler, 2007: Expansion of the Hadley cell under global warming. *Geophys. Res. Lett.*, **34**, L06805, https://doi.org/10.1029/2006GL028443.

Ma, J., and S. P. Xie, 2013: Regional patterns of sea surface temperature change: A source of uncertainty in future projections of precipitation and atmospheric circulation. *J. Climate*, **26**, 2482–2501, https://doi.org/10.1175/JCLI-D-12-00283.1.

McVicar, T. R., and Coauthors, 2012: Global review and synthesis of trends in observed terrestrial near-surface wind speeds: Implications for evaporation. *J. Hydrol.*, **416–417**, 182–205, https://doi.org/10.1016/j.jhydrol.2011.10.024.

Medvigy, D., R. L. Walko, M. J. Otte, and R. Avissar, 2013: Simulated changes in northwest U.S. climate in response to Amazon deforestation. *J. Climate*, **26**, 9115–9136, https://doi.org/10.1175/JCLI-D-12-00775.1.

Milly, P. C. D., 1992: Potential evaporation and soil moisture in general circulation models. *J. Climate*, **5**, 209–226, https://doi.org/10.1175/1520-0442(1992)005<0209:PEASMI>2.0.CO;2.

Neale, R.B., and Coauthors, 2012: Description of the NCAR Community Atmosphere Model (CAM 5.0). NCAR Tech. Note NCAR/TN-486+STR, 274 pp., www.cesm.ucar.edu/models/cesm1.0/cam/docs/description/cam5_desc.pdf.

Oleson, K.W., and Coauthors, 2010: Technical description of version 4.0 of the Community Land Model (CLM). NCAR Tech. Note NCAR/TN-478+STR, 257 pp., https://doi.org/10.5065/D6FB50WZ.

Puma, M. J., and B. I. Cook, 2010: Effects of irrigation on global climate during the 20th century. *J. Geophys. Res.*, **115**, D16120, https://doi.org/10.1029/2010JD014122.

Santanello, J. A., and Coauthors, 2018: Land–atmosphere interactions the LoCo perspective. *Bull. Amer. Meteor. Soc.*, **99**, 1253–1272, https://doi.org/10.1175/BAMS-D-17-0001.1.

Schneck, R., and V. Mosbrugger, 2011: Simulated climate effects of Southeast Asian deforestation: Regional processes and teleconnection mechanisms. *J. Geophys. Res.*, **116**, D11116, https://doi.org/10.1029/2010JD015450.

Seager, R., N. Harnik, Y. Kushnir, W. Robinson, and J. Miller, 2003: Mechanisms of hemispherically symmetric climate variability. *J. Climate*, **16**, 2960–2978, https://doi.org/10.1175/1520-0442(2003)016<2960:MOHSCV>2.0.CO;2.

Seneviratne, S. I., and Coauthors, 2006: Soil moisture memory in AGCM simulations: Analysis of Global Land–Atmosphere Coupling Experiment (GLACE) data. *J. Hydrometeor.*, **7**, 1090–1112, https://doi.org/10.1175/JHM533.1.

——, T. Corti, E. L. Davin, M. Hirschi, E. B. Jaeger, I. Lehner, B. Orlowsky, and A. J. Teuling, 2010: Investigating soil moisture–climate interactions in a changing climate: A review. *Earth-Sci. Rev.*, **99**, 125–161, https://doi.org/10.1016/j.earscirev.2010.02.004.

Seo, K. H., D. M. W. Frierson, and J. H. Son, 2014: A mechanism for future changes in Hadley circulation strength in CMIP5 climate change simulations. *Geophys. Res. Lett.*, **41**, 5251–5258, https://doi.org/10.1002/2014GL060868.

Shukla, J., and Y. Mintz, 1982: Influence of land-surface evapotranspiration on the Earth's climate. *Science*, **215**, 1498–1501, https://doi.org/10.1126/science.215.4539.1498.

Snyder, P. K., 2010: The influence of tropical deforestation on the Northern Hemisphere climate by atmospheric teleconnections. *Earth Interact.*, **14** (4), 1–34, https://doi.org/10.1175/2010EI280.1.

Swann, A. L. S., I. Y. Fung, and J. C. H. Chiang, 2012: Mid-latitude afforestation shifts general circulation and tropical precipitation. *Proc. Natl. Acad. Sci. USA*, **109**, 712–716, https://doi.org/10.1073/pnas.1116706108.

Trenberth, K. E., and D. P. Stepaniak, 2003: Seamless poleward atmospheric energy transports and implications for the Hadley circulation. *J. Climate*, **16**, 3706–3722, https://doi.org/10.1175/1520-0442(2003)016<3706:SPAETA>2.0.CO;2.

Walker, J., and P. R. Rowntree, 1977: The effect of soil moisture on circulation and rainfall in a tropical model. *Quart. J. Roy. Meteor. Soc.*, **103**, 29–46, https://doi.org/10.1002/qj.49710343503.

Walker, J. M., and S. Bordoni, 2016: Onset and withdrawal of the large-scale South Asian monsoon: A dynamical definition using change point detection. *Geophys. Res. Lett.*, **43**, 11 815–11 822, https://doi.org/10.1002/2016GL071026.

Wang, F., A. Ducharne, F. Cheruy, M. H. Lo, and J. Y. Grandpeix, 2018: Impact of a shallow groundwater table on the global water cycle in the IPSL land–atmosphere coupled model. *Climate Dyn.*, **50**, 3505–3522, https://doi.org/10.1007/s00382-017-3820-9.

Webster, P. J., and S. Yang, 1992: Monsoon and ENSO: Selectively interactive systems. *Quart. J. Roy. Meteor. Soc.*, **118**, 877–926, https://doi.org/10.1002/qj.49711850705.

Werth, D., 2002: The local and global effects of Amazon deforestation. *J. Geophys. Res.*, **107**, 8087, https://doi.org/10.1029/2001JD000717.

Williamson, D. L., and Coauthors, 2013: The Aqua-Planet Experiment (APE): Response to changed meridional SST profile. *J. Meteor. Soc. Japan*, **91A**, 57–89, https://doi.org/10.2151/jmsj.2013-A03.

Wu, Y., M. Ting, R. Seager, H.-P. Huang, and M. A. Cane, 2010: Changes in storm tracks and energy transports in a warmer climate simulated by the GFDL CM2.1 model. *Climate Dyn.*, **37**, 53–72, https://doi.org/10.1007/s00382-010-0776-4.

Yano, J. I., 1998: An aquaplanet monsoon. *J. Atmos. Sci.*, **55**, 1373–1399, https://doi.org/10.1175/1520-0469(1998)055<1373:AAM>2.0.CO;2.

Yeh, T. C., R. T. Wetherald, and S. Manabe, 1984: The effect of soil moisture on the short-term climate and hydrology change—A numerical experiment. *Mon. Wea. Rev.*, **112**, 474–490, https://doi.org/10.1175/1520-0493(1984)112<0474:TEOSMO>2.0.CO;2.

York, J. P., M. Person, W. J. Gutowski, and T. C. Winter, 2002: Putting aquifers into atmospheric simulation models: An example from the Mill Creek watershed, northeastern Kansas. *Adv. Water Resour.*, **25**, 221–238, https://doi.org/10.1016/S0309-1708(01)00021-5.

Zeng, X., and M. Decker, 2009: Improving the numerical solution of soil moisture–based Richards equation for land models with a deep or shallow water table. *J. Hydrometeor.*, **10**, 308–319, https://doi.org/10.1175/2008JHM1011.1.